Additive Manufacturing: Metallurgy, Cut Analysis & Porosity

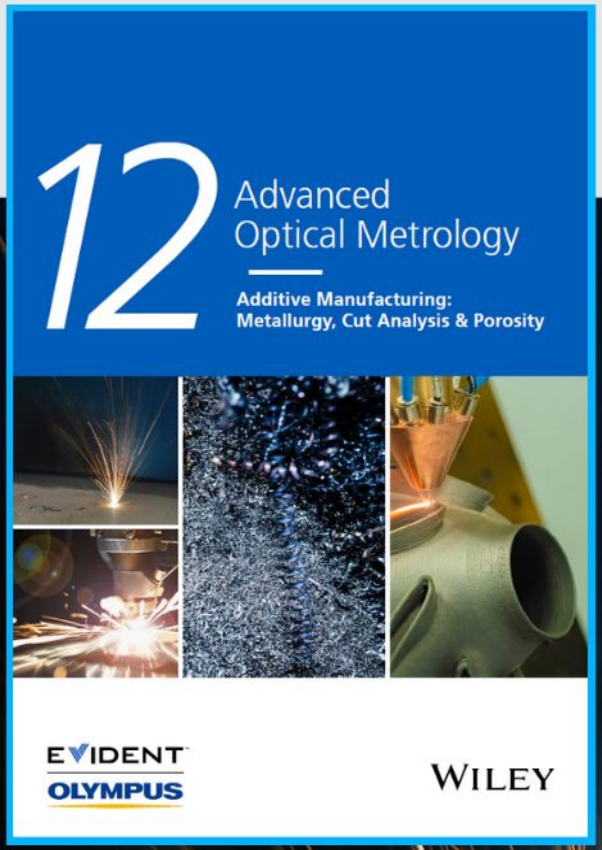

The latest eBook from Advanced Optical Metrology. Download for free.

In industry, sector after sector is moving away from conventional production methods to additive manufacturing, a technology that has been recommended for substantial research investment.

Download the latest eBook to read about the applications, trends, opportunities, and challenges around this process, and how it has been adapted to different industrial sectors.

EVIDENT
OLYMPUS

WILEY

Heteroepitaxy

Heteroepitaxial Growth of Nanoscale Oxide Shell/Fiber Superstructures by Mild Hydrothermal Processes**

*Chun-Hu Chen, Lei Jin, Anais E. Espinal, Brian T. Firliet, Linping Xu, Mark Aindow, Raymond Joesten, and Steven L. Suib**

For many crystalline nanomaterials, the physical and chemical properties of interest are dictated by the crystal structure that they adopt and, more specifically, by the orientation of the surface facets that they exhibit. Thus, the specific crystalline faces exposed are important in catalytic reactions, absorption of light, mechanical strength, sensing, and many other types of behavior.[1–4] The controlled synthesis of nanoparticulate materials with specific structures, morphologies, and orientations is, however, particularly challenging. Most of the reported methods require complicated procedures, surfactants/templates, or expensive instrumentation to produce nanoscale arrays, and some materials have defied all attempts at controlled growth.

The materials that has attracted the most attention is titania; this is one of the most important oxides used in photocatalysis, paints, and pigments. Nanostructured TiO_2 materials have been reported to exhibit interesting properties and could play a pivotal role in next-generation solar cells and other energy-harvesting technologies.[5] Unfortunately, despite the extensive range of different approaches that have been explored for the controlled synthesis of nanostructured TiO_2, the level of structural and morphological control required for certain device applications has not yet been achieved.

In this work we explore the use of epitaxial growth to obtain structure and orientation selective synthesis of nanostructured TiO_2. In this approach one could use a substrate material with appropriate lattice parameters for the oriented deposition of rutile (the desired phase of titania), and for which the morphological and orientational control during nanomaterial synthesis is known to be more straightforward than for TiO_2. The substrate material chosen for these studies is manganese dioxide, which exists in a wide range of different polymorphic crystal structures including tunnel, layer, and three-dimensional (3D) framework structures. All of these MnO_2 structures have some lattice periodicities similar to those of rutile TiO_2 and could thus serve as appropriate substrate materials. Moreover, these MnO_2 materials can be produced as nanoscale architectures with exceptional control of structure, morphology, and orientation using simple redox, solvothermal, or hydrothermal processes under mild conditions.[6–10] These scalable processes have already been developed to enable the structural and chemical properties of the MnO_2 nanomaterials to be exploited in adsorption, batteries, catalysis, sensors, and so on.

Here we report the successful heteroepitaxy for rutile TiO_2 onto a nanostructured MnO_2 substrate using an inexpensive, single-step hydrothermal procedure under mild conditions. The key factor in this process is the use of $TiOSO_4$ as the titania precursor. More conventional titania precursors, such as $TiCl_4$ or $Ti(OR)_4$ in organic solvents, are not suitable for heteroepitaxial growth in aqueous solution because they undergo extremely rapid hydrolysis in the presence of moisture; this leads to a high nucleation rate and the formation of randomly oriented titania nuclei. The $TiOSO_4$ precursor allows for thermal control of hydrolysis in a pure aqueous phase facilitating low-temperature heteroepitaxial growth via a hydrothermal reaction.

The substrate used comprised microspherical aggregates of single-crystal MnO_2 needles with the cryptomelane structure (also known as octahedral molecular sieve 2 or OMS-2),[6] and the heteroepitaxy resulted in a unique nanoscale shell/fiber superstructure (NSFS), a complex structure composed of nanoscale coating shell and nanofiber arrays. The hydrothermal synthesis of the microspherical cryptomelane MnO_2 substrate material has been described elsewhere,[9] and a secondary-electron (SE) scanning electron microscopy (SEM) image of

[*] Prof. S. L. Suib, C.-H. Chen, L. Jin, B. T. Firliet, L.-P. Xu, Prof. R. Joesten
Department of Chemistry
University of Connecticut
55 North Eagleville Road, Storrs, CT 06269–3060 (USA)
E-mail: steven.suib@uconn.edu
Prof. M. Aindow
Department of Chemical, Materials & Biomolecular Engineering
University of Connecticut
55 North Eagleville Road, Storrs, CT 06269 (USA)
Prof. M. Aindow, Prof. S. L. Suib, A. E. Espinal
Institute of Materials Science
University of Connecticut
55 North Eagleville Road, Storrs, CT 06269 (USA)

[**] We acknowledge the support of the U.S. Department of Energy, Office of Basic Energy Sciences, Division of Chemical Sciences, Geosciences, and Biosciences for support of this research. We thank the Center for Environmental Sciences and Engineering of the University of Connecticut for support and assistance in executing the research. We also thank Dr. Frank Galasso, Dr. Xiongfei Shen, and Mr. Shih-Po Sun for helpful discussions and suggestions.

Supporting Information is available on the WWW under http://www.small-journal.com or from the author.

DOI: 10.1002/smll.200902381

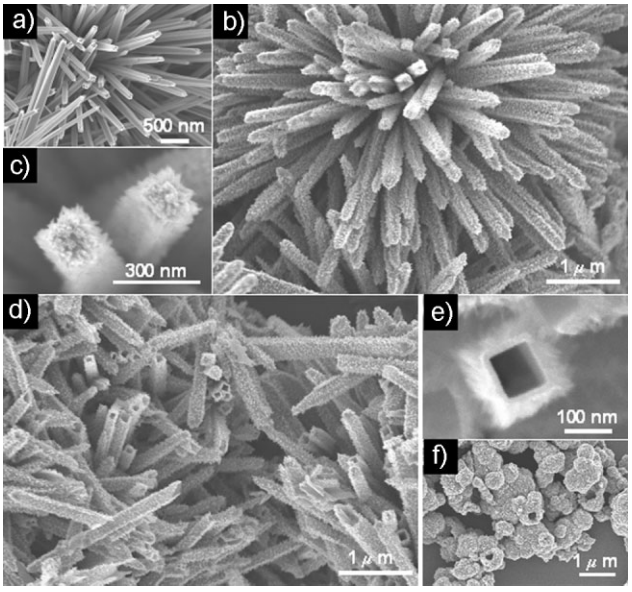

Figure 1. SE SEM images of TiO_2 NSFS. a) The pure microspherical cryptomelane MnO_2 substrate before processing; b) TiO_2/MnO_2 NSFS after processing; c) higher-magnification view of (b) showing the surface nanofibers; d) free-standing nanoscale tubular TiO_2 superstructure after acid treatment to remove the MnO_2 substrate; e) higher-magnification view of (d) showing that the square cross-section tubular structure has an empty core corresponding to the size and shape of the substrate needles in (a); f) irregular anatase TiO_2 particles from the control experiment without an MnO_2 substrate.

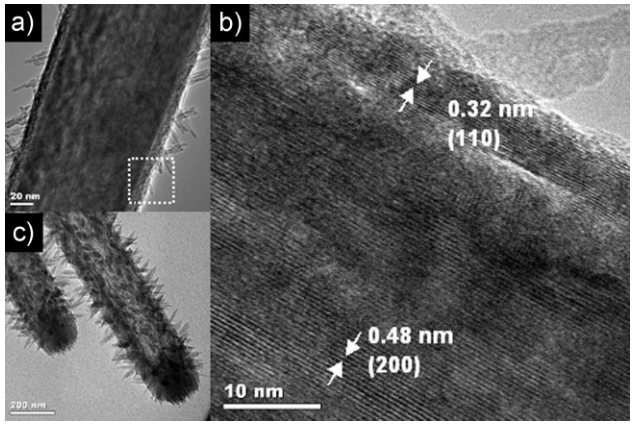

Figure 2. TEM images obtained from the TiO_2 NSFS deposits on microspherical cryptomelane MnO_2: a) projection through a TiO_2-coated MnO_2 needle, showing the heteroepitaxial interface and the core/shell structure; b) high-resolution image of the area indicated by the white square in (a) – the spacings of the fringes parallel to the interface in the substrate (0.48 nm) and the shell (0.32 nm) correspond to those for (200) in cryptomelane MnO_2 and (110) in rutile TiO_2, respectively; c) rutile TiO_2 NSFS after the substrate removal, showing a hollow tubular structure with parallel surface fibers.

the material is shown in Figure 1a. This material was selected as the substrate for the current study for the following reasons: the constituent needles have a convenient thickness (<100 nm) for direct examination by transmission electron microscopy (TEM), the square cross section of the needles is useful to evaluate the surface and edge coverage of the TiO_2 deposit, and the cryptomelane MnO_2 substrate can be removed readily using a weak organic acid resulting in hollow NSFS rutile TiO_2.

The SE SEM images obtained from the coated cryptomelane MnO_2 (Figure 1b) reveal that the coating is uniform and replicates the overall morphology of the substrate needles, although higher-magnification images (Figure 1c) reveal the presence of nanoscale fibers protruding from the surface. The uniformity of the inner shell of this NSFS is revealed more clearly in SE SEM images from the material after acid removal of the MnO_2 substrate (Figure 1d and e). The resultant hollow NSFS comprised a uniform 25-nm-thick shell that conforms to the square morphology of the removed cryptomelane MnO_2 needles, with 5–10-nm-thick fibers emanating from the shell surface, rather than that of the substrate. We note that the hollow NSFS exhibits good structural integrity with no evidence of shell collapse after the removal of the supporting MnO_2 substrate.

The X-ray diffraction (XRD) data obtained from this NSFS show that the TiO_2 phase present is rutile (Supporting Information, Figure S2). These data are very different from those obtained in control experiments wherein TiO_2 was produced using the same reagents and rotary hydrothermal treatment without any MnO_2 substrate. The SE SEM images (Figure 1f) show that relatively coarse (≈1 μm) spherical particles were obtained and the XRD data reveal that these are composed of the anatase polymorph of TiO_2 (Supporting Information, Figure S3). Since anatase is the equilibrium low-temperature phase of TiO_2, the adoption of the rutile structure by the TiO_2 in the NSFS grown in our studies is the result of structural templating by the cryptomelane MnO_2 substrate via heteroepitaxial growth, as discussed below.

To investigate the morphological development in these NSFS, further deposition experiments were performed using different $TiOSO_4$ solution concentrations giving corresponding changes in deposit thickness (see Supporting Information). The SE SEM images in Figure S4 of the Supporting Information show that the deposits formed using dilute (1.25 mM) solutions are shells upon the cryptomelane MnO_2 needles with no nanofiber protrusions, whereas increasing the solution concentration leads to an increase in both the length and density of the nanofibers. These observations indicate that the formation of the TiO_2 shell takes place prior to the generation of surface nanofibers in this superstructure.

Further evidence for the influence of the substrate was obtained in transmission electron microscopy (TEM) images of the NSFS material. Images through individual coated cryptomelane MnO_2 needles (Figure 2a) together with energy-dispersive X-ray spectrometry (EDXS) data (Supporting Information, Figure S5) confirm that the TiO_2 is composed of a thin contiguous shell on the cryptomelane MnO_2 surface with nanofibers emanating from the outer surface of the shell. High-resolution TEM images (Figure 2b) of the MnO_2/TiO_2 interface show that this is abrupt and heteroepitaxial with (100) in the cryptomelane MnO_2 parallel to (110) in the TiO_2 shell. Images of the material produced by acid removal of the core (Figure 2c) show that the features of the TiO_2 in the NSFS are preserved. The absence of a Mn Kα signal in the EDXS data

from such regions (Supporting Information, Figure S6b) confirms that the removal of the MnO_2 is complete.

From an analysis of high-resolution TEM images such as Figure 2b and the corresponding selected-area diffraction data (SAED; see Supporting Information, Figure S7), it was found that the rutile TiO_2 shell adopts the following epitaxial orientation relationship (OR) with respect to the cryptomelane MnO_2 core:

$$(100)_{\text{Cryptomelane}}//(110)_{\text{Rutile}}$$

$$[010]_{\text{Cryptomelane}}//[1\bar{1}0]_{\text{Rutile}}$$

$$[001]_{\text{Cryptomelane}}//[001]_{\text{Rutile}}$$

In this OR, the directions $[010]_{\text{Cryptomelane}}$ and $[001]_{\text{Cryptomelane}}$ correspond to the major and minor axes, respectively, of the cryptomelane MnO_2 needle lying parallel to the heteroepitaxial interface. For cryptomelane MnO_2 with $a_0 = 0.982$ nm and $c_0 = 0.285$, and rutile TiO_2 with $a_0 = 0.459$ nm and $c_0 = 0.296$, the misfit along the minor axis is 3.86%. The nominal misfit along the major axis is much larger (−33.9%) but if one considers the formation of a supercell in which $3[110]_{\text{Rutile}}$ matches $2[010]_{\text{Cryptomelane}}$ then this value falls dramatically to −0.86%. Since the basic structural units for both cryptomelane and rutile are octahedral with transition metal atoms at the centers and oxygen atoms at the apices, the rectangular motif for this superstructure parallel to the interface plane can be represented most easily by plotting the transition metal atom positions, as shown in Supporting Information, Figure S8. In addition to the formation of a low-misfit motif, it can be seen that this superstructure would arise naturally from the arrangement of the octahedral structural units in a (001) cross section through the epitaxial interface, as shown in Figure 3. In this section the [001] projection of the cryptomelane structure on the left of the image reveals the 2×2 and 1×1 tunnels, and the most likely position for the terminating plane on the (100) surface of the needle would be that that bisects both tunnel types as indicated. If TiO_6 octahedra were to deposit on this surface and complete the 1×1 tunnels, then the addition of octahedra in the bridging positions to complete the plane would only require a distortion of −0.86% along [010], and this would correspond to the formation of the superstructure as described above. In the subsequent deposition of TiO_2 the additional sheets of such octahedra would constitute (110) planes in the rutile structure with arrays of 1×1 tunnels parallel to [001], as shown on the right of the image.

The formation of this low-misfit interface structure is presumably what leads to the stabilization of the rutile phase of TiO_2, rather than the equilibrium anatase polymorph. We note, however, that the elastic constants for oxide ceramics such as rutile are very high and so one would not expect that a pseudomorphic epitaxial deposit could be maintained to significant shell thicknesses even though the magnitudes of the elastic strains required are modest. To illustrate this point we have used a standard Matthews–Blakeslee analysis[11] to calculate the critical thickness, h_c, at which one would expect the energy of a pseudomorphic epitaxial deposit to exceed that of a semicoherent deposit where the misfit strains were

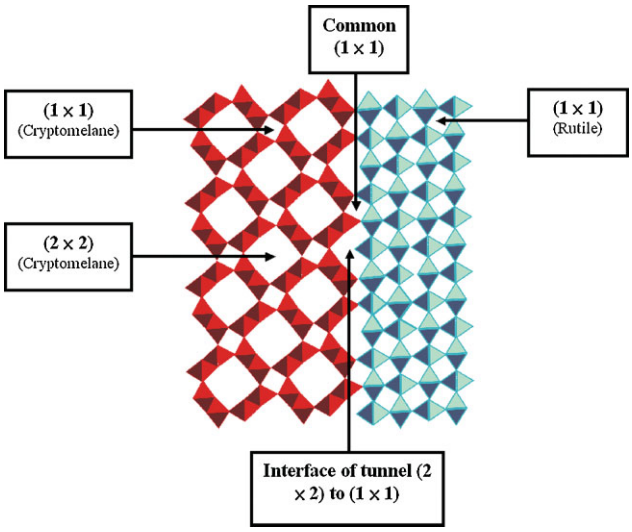

Figure 3. Schematic [001] projection (i.e., parallel to the MnO_2 needle axis) of the heteroepitaxial interface formed between cryptomelane MnO_2 and rutile TiO_2. The arrangement of the red MnO_6 octahedra on the left of the figure defines the mixture of 1×1 and 2×2 tunnels in the cryptomelane structure. The arrangement of these octahedral on the vertical (100) surface of the MnO_2 acts as a structural template for the TiO_6 octahedra (blue) during deposition, leading to the adoption of the rutile structure with 1×1 tunnels as shown, rather than the equilibrium anatase polymorph TiO_2.

balanced by interfacial misfit dislocations. Taking the misfit components of −0.86% and 3.86% in the interface plane, we obtain $h_c = 70$ and 11 nm, respectively (see Supporting Information). While the introduction of misfit dislocations by glide processes as envisioned by Matthews and Blakeslee is unlikely in these systems due to the lack of dislocation sources and the very low dislocation mobilities in such oxides at the growth temperature, the values of h_c obtained do give some indication of the thickness at which the pseudomorphic deposit would be energetically unfavorable. We note that in all of the rutile NSFS produced in this study, the shell thicknesses lie between these values. Thus, the transition from a uniform shell to the NSFS structure could be driven by an alternate relaxation mechanism such as the development of surface ripple, as described by Cullis et al.[12] Once such a morphological instability developed, it could readily lead to the formation of nucleation sites for secondary deposits, which would develop into unconstrained nanofiber protrusions as observed experimentally.

We note that the morphology of the nanofiber protrusions on the titania shell may also represent a further opportunity for the exploitation of such materials. Since the majority of the surface nanofibers are oriented at characteristic angles to the titania shell (≈60–65°) in a nanoscale antenna-like morphology, they may have significant potential in the area of solar energy devices and photocatalysis. As shown in Figure 4a, the cryptomelane MnO_2 array thin films were first obtained by pulsed laser deposition (PLD) on (001) strontium titanate (STO) substrates.[13] The TiO_2 coating procedure with proper precursor concentrations was then applied to the MnO_2/STO substrates.[14] The products show a homogeneous TiO_2 nanoscale superstructure coating with large-scale (centimeter)

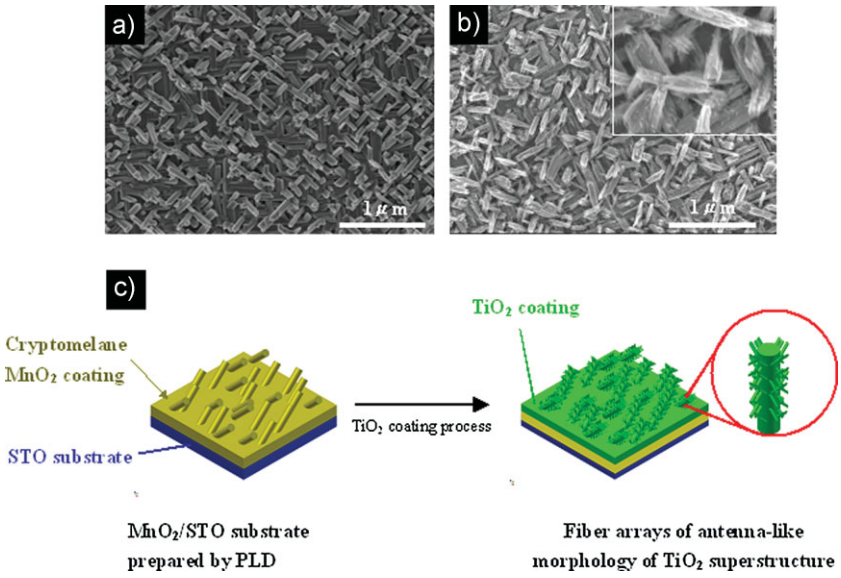

Figure 4. Rutile TiO_2 superstructure on MnO_2/STO substrates: a,b) SE SEM images of the cryptomelane MnO_2 thin film deposited by PLD onto a (001) STO substrate, and the rutile TiO_2-coated MnO_2 thin film, respectively; c) schematic diagram showing how the coating process leads to the formation of antenna-like morphologies in arrays suitable for energy-harvesting or sensor devices.

coverage, demonstrating the generality of this method for a range of length scales, rather than just the nanoscale (Figure 4 and Supporting Information, Figure S9). With the unique antenna-like morphology of the arrays and the ability to form large-scale coatings using such mild conditions, such heteroepitaxial growth could be a promising route to produce materials for numerous light-harvesting technologies or devices, particularly for dye-sensitized solar cells (DSSCs), nanogenerators, water oxidation, and sensors.[1–3,15,16]

These results represent a proof-of-principle demonstration of the ability to produce epitaxial core/shell structures and derivative hollow structures using mild hydrothermal processes. The general applicability of this heteroepitaxial relationship and approach was evaluated by attempting to deposit other metal oxides with similar crystal structures using the same procedure. Preliminary data obtained from SnO_2 deposits on the same cryptomelane MnO_2 substrate material show that a similar uniform shell is formed but with more disordered nanoparticulate surface features (Supporting Information, Figure S10). This presumably occurs because SnO_2 is isostructural with rutile but has larger lattice parameters ($a_0 = 0.474$ nm and $c_0 = 0.319$) leading to larger lattice misfits at the interface as the OR given above the misfits are 11.9% and 2.4% on the minor and major axes, respectively. The 11.9% misfit is much larger than that of the SnO_2/α-Fe_2O_3 interface reported by Zhang et al.,[17] and would give much higher elastic-strain energies in the pseudomorphic deposits, leading to more profound morphological instability effects.

In summary, a general heteroepitaxy under mild hydrothermal conditions has been developed successfully to produce nanoscale shape-controlled superstructures and derivative hollow structures of rutile TiO_2 and related oxides. The simplicity of this method means that it could be adapted easily to various combinations of other metal oxide substrates and other coated oxides. The application to tunnel structure oxides is particularly interesting and further studies are underway. These will include the possibilities of 3×3 to 1×1, 3×3 to 2×2, 2×2 to $1 \times$ infinite layered structures[18] or even 3×2 to 2×1, 4×3 to 3×2, 5×4 to 4×3, and so on, with different elements, such as other rutile materials (CrO_2, IrO_2, GeO_2, etc.)[19] and substrates (2×2 for akaganeite (FeO (OH)) and ankangite $Ba(Ti,V)_8O_{16}$ and/or other possible species).[20,21] These studies will provide helpful information to understand and lead the design of controlled growth processes for diverse nanoscale superstructures of various materials.

Experimental Section

Preparation of TiO_2 nanoscale shell/fiber superstructure: 10 mg of as-synthesized microspherical cryptomelane MnO_2 was mixed with 13 mL of $TiOSO_4$ solution (2.5 mM) in H_2SO_4 (0.1 M) solution; the mixture was then transferred to a 23 mL Teflon-lined autoclave and reacted at 100 °C for 1 day using a rotary hydrothermal treatment. The product was rinsed with DI water and dried at 100 °C for 12 h. To remove the cryptomelane MnO_2 substrate, the as-obtained TiO_2-coated materials were mixed with 10 mL of saturated oxalic acid solution at 70 °C for 5 min, followed by rinsing with DI water several times to remove the excess oxalic acid.

Preparation of SnO_2 superstructure: 5 mL of 0.3 M $SnCl_4 \cdot 5H_2O$ solution was added to 100 mL of 0.15 M KOH solution and stirred overnight to obtain a clear solution. 13 mL of this solution was mixed with 10 mg of the microspherical cryptomelane MnO_2; the mixture was then transferred to a 23 mL Teflon-lined autoclave and reacted at 180 °C for 1 day using a rotary hydrothermal treatment. The process for the removal of cryptomelane MnO_2 substrate is the same as for the TiO_2 NSFS.

Characterization: XRD characterization was performed using a Scintag PDS 2000 diffractometer with a CuKα X-ray source. High-resolution TEM images were obtained in a JEOL JEM 2010 FasTEM equipped with an energy-dispersive X-ray detector. Field-emission SEM studies were carried out using a Zeiss DSM 982 Gemini FESEM.

Keywords:

cryptomelane · heteroepitaxy · nanostructures · rutile

[1] N. S. Lewis, *Science* **2007**, *315*, 798.
[2] Z. L. Wang, J. Song, *Science* **2006**, *312*, 242.
[3] A. P. Goodey, S. M. Eichfeld, K.-K. Lew, J. M. Redwing, T. E. Mallouk, *J. Am. Chem. Soc.* **2007**, *129*, 12344.
[4] N. Tian, Z.-Y. Zhou, S.-G. Sun, Y. Ding, Z. L. Wang, *Science* **2007**, *316*, 732.
[5] X. Chen, S. S. Mao, *Chem. Rev.* **2007**, *107*, 2891.

[6] S. L. Suib, *Acc. Chem. Res.* **2008**, *41*, 479.
[7] W.-N. Li, L. Zhang, S. Sithambaram, J. Yuan, X.-F. Shen, M. Aindow, S. L. Suib, *J. Phys. Chem. C* **2007**, *111*, 14694.
[8] J. Yuan, K. Laubernds, J. Villegas, S. Gomez, S. L. Suib, *Adv. Mater.* **2004**, *16*, 1729.
[9] J. Yuan, W.-N. Li, S. Gomez, S. L. Suib, *J. Am. Chem. Soc.* **2005**, *127*, 14184.
[10] C.-H. Chen, V. M. B. Crisostomo, W.-N. Li, L. Xu, S. L. Suib, *J. Am. Chem. Soc.* **2008**, *130*, 14390.
[11] J. W. Matthews, A. E. Blakeslee, *J. Cryst. Growth* **1974**, *27*, 118.
[12] A. G. Cullis, D. J. Robbins, S. J. Barnett, A. J. Pidduck, *J. Vac. Sci. Technol. A* **1994**, *12*, 1924.
[13] A. E. Espinal, L. Zhang, C.-H. Chen, A. Morey, Y. Nie, L. Espinal, B. O. Wells, R. Joesten, M. Aindow, S. L. Suib, *Nat. Mater.* **2009**, *9*, 54.
[14] The as-prepared MnO_2/STO film (1 cm × 1 cm) was placed in a Teflon liner autoclave upside down, followed by the addition of 10 mL of 8 mM $TiOSO_4$ precursor solution. The whole liner was sealed in an autoclave and then reacted at 100 °C for 1 day by hydrothermal treatment.
[15] G. K. Mor, K. Shankar, M. Paulose, O. K. Varghese, C. A. Grimes, *Nano Lett.* **2006**, *6*, 215.
[16] R. Nakamura, T. Okamura, N. Ohashi, A. Imanishi, Y. Nakato, *J. Am. Chem. Soc.* **2005**, *127*, 12975.
[17] D.-F. Zhang, L.-D. Sun, C.-J. Jia, Z.-G. Yan, L.-P. You, C.-H. Yan, *J. Am. Chem. Soc.* **2005**, *127*, 13492.
[18] D. Portehault, S. Cassaignon, E. Baudrin, J.-P. Jolivet, *Chem. Commun.* **2009**, 674.
[19] F. Galasso, *Structure and Properties of Inorganic Solids*, Pergamon Press, New York, **1970**.
[20] M. Pasero, *Rev. Mineral. Geochem.* **2005**, *57*, 291.
[21] J. Zhang, C. W. Burnham, *Am. Mineral.* **1994**, *79*, 168.

Received: December 24, 2009